26th Optoelectronics and Communications Conference (OECC)
2021 © OSA 2021

Recent progress in quantum dot distributed feedback lasers with large wavelength detuning for uncooled and isolation-free applications

F. Grillot[1,2], B. Dong[1], J. Liu[1], H. Huang[1], K. Nishi[3], K. Takemasa[3], M. Sugawara[3], and J. E. Bowers[4,5]

[1)] LTCI, Télécom Paris, Institut Polytechnique de Paris, 19 Place Marguerite Perey, 91120 Palaiseau, France
[2)] Center for High Technology Materials, University of New-Mexico, Albuquerque, New-Mexico, 87106, USA
[3)] QD Laser, Inc., Kawasaki, Kanagawa 210-0855, Japan
[4)] Institute for Energy Efficiency, University of California, Santa Barbara, California 93106, USA
[5)] Materials Department, University of California, Santa Barbara, California 93106, USA
frederic.grillot@telecom-paris.fr

Abstract: This work reports on the temperature performance of a 1.3-micron InA/GaAs quantum dot distributed feedback laser operating with a large optical wavelength detuning. Isolator-free transmission with pulse amplitude modulation is achieved under strong optical feedback.

OCIS codes: 250.5960, 140.3490, 250.5590.

1. Introduction

With the development of 5G and artificial intelligence, data centers are becoming the mainstream for carriers networks and service systems. However, because of the large amount of data circulating across the optical networks, the power consumption of the data centers is currently increasing worldwide [1]. This severe drawback can significantly be solved thanks to silicon photonics that is a powerful technology for energy efficiency as well as for the miniaturization and integration of a wide range of optoelectronic components such as modulators, waveguides, and laser sources [2]. In the latter, quantum dots (QDs) lasers made with zero-dimensional nanostructures enable high performance photonic devices with low threshold currents and high level of feedback tolerance [3,4] hence making them ideal for the aforementioned applications. This work goes a step beyond in the improvement of InAs/GaAs QD devices and shows newest results with a distributed feedback (DFB) laser structure. Here, we demonstrate that the utilization of QD nanostructures as an active gain medium together with a large optical wavelength detuning (OWD) between the lasing peak (DFB) and the gain peak [5] allows to strongly control the device performance over temperature. In particular, we show that the QD DFB laser enables the best static, dynamic and nonlinear performance at high temperatures. For example, floor-free transmission is achieved with strong feedback under pulse amplitude modulation (PAM) at 55°C. Overall, the results are of paramount importance for isolator-free applications as well as for emerging markets requiring high temperature operations and improved coherent light sources, such as resource findings in deep underground, mobile applications, and uncooled integrated system.

2. Device structure

The active region of the device is grown from 8-layer InAs QDs on (100) GaAs substrate by using molecular beam epitaxy. The density of QDs is $\sim 6 \times 10^{10}$ cm^{-2} per layer. Each dot layer was separated by a p-doped GaAs spacer, hence providing a modal gain up of about 50 to 60 cm^{-1}. The corrugated structure above the active region is fabricated with electron beam lithography and wet etching, the InGaP/GaAs gratings on top are formed by metal organic vapour phase epitaxy. The normalized coupling coefficient κL of the DFB laser is 1.2 which allows a fine control the longitudinal spatial hole burning. The laser is designed to operate at a high temperature and the OWD between the gain peak and the lasing oscillation is fixed at 25 nm at 25°C. Finally, in order to ensure a single mode operation with large output power, a high-reflection coating (HR) is applied on the rear facet while the front one is antireflection coated (AR). A schematic view of the laser design is displayed in inset of Fig. 1(a). More details about the epitaxial structure and device fabrication process are available elsewhere [6].

3. Static characteristics

Figure 1(a) depicts the light-current (L-I) of the QD DFB laser for different temperature conditions. With the increase of temperature from 15 to 55°C, the device exhibits a high level of stability against the temperature variation, by maintaining a sufficient output power over 15 mW. Interestingly, the threshold current I_{th} is largely reduced from 10.6 down to 6 mA with the increase of temperature from 15 to 55°C, as shown in Fig. 1(b). An empirical law predicts the changes in threshold current, I_{th} such as $I_{th} \propto e^{T/T_0}$ with T_0 the characteristic temperature parameter describing the device's sensitivity to a change in junction temperature ΔT. The QD laser under study

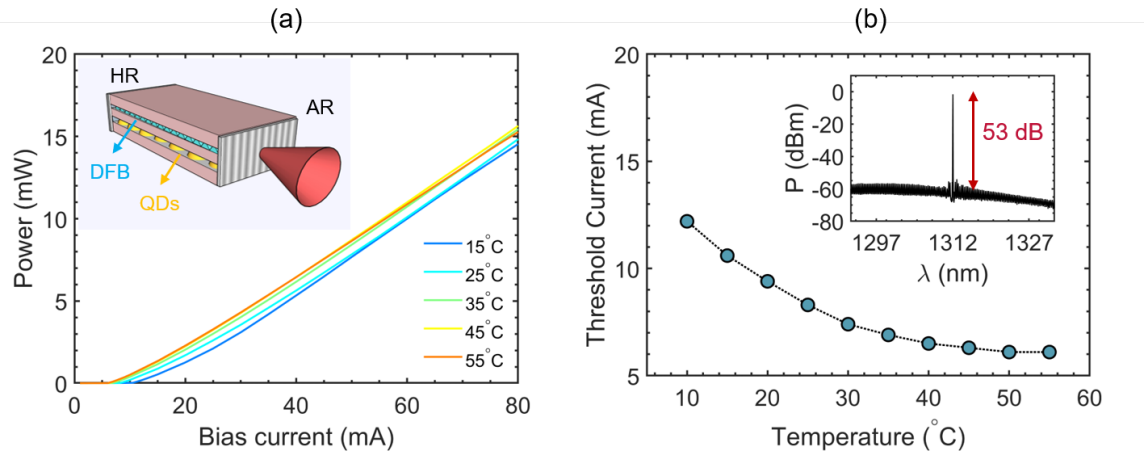

Fig. 1. (a) Light-current characteristics and (b) Threshold current with temperature varying from 15 to 55°C. The inset displays the optical spectrum at 55°C with a SMSR of 53 dB

.

does not show such exponential behavior of its threshold current with temperature. Let us stress that the same feature is observed on the external efficiency (not shown here). Also, the optical spectrum measured at 55°C above the threshold and displayed in the inset of Figure 1(b) confirms the strong single mode behavior with a side mode suppression ratio (SMSR) as high as 53 dB.

4. Modulation dynamics

Fig. 2(a) depicts the damping factor γ as a function of the squared relaxation oscillation frequency f_{RO} at 20°C (gray) and at 55°C (jade). The linear evolution marked in the same color is defined as $\gamma = Kf_{RO}^2 + \gamma_0$ with K the K-factor and γ_0 the damping factor offset. The K-factor is used to extract the maximum 3-dB modulation bandwidth through $f_{3dB,max} = 2\sqrt{2}\pi/K$. In Fig. 2(b), we observe a decrease of the K-factor from 2.87 to 1.72 ns with increasing temperature from 20 to 55°C. This reduction of the K-factor with temperature is attributed to the large optical mismatch used in this single frequency DFB laser.

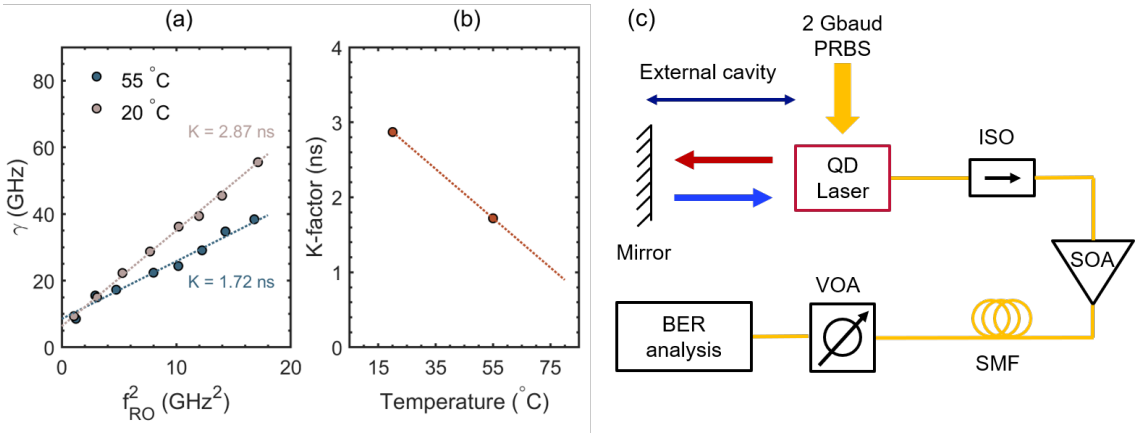

Fig. 2. (b) Damping factor γ as a function of the squared relaxation oscillation frequency f_{RO}^2 at different temperatures. (b) Tendency of the K-factor versus the temperature. (c) Apparatus of the test-bed experiment. ISO: optical isolator; SOA: semiconductor optical amplifier; SMF: 12 km long single mode fiber coil; VOA: variable optical attenuator.

5. Pulse amplitude modulation

Fig. 2(c) displays the experimental configuration for the PAM modulation experiments. The laser is directly modulated by a pulse amplitude modulation 4-level (PAM4) signal with pseudo-random binary sequence (PRBS) and a bit sequence length of $2^{31} - 1$. 90% of the laser output is sent to a 12 m-long external cavity, at the end of which

a mirror is used to reflect the light back to the laser cavity. In the transmission configuration, the remaining 10% of power is then preamplified and propagated through a 12 km single-mode fiber (SMF). In the end, a variable optical attenuator (VOA) is used to change the received power of the error detector to characterize the bit-error-rate (BER) performance. The operation temperature is kept at 55°C for which the laser's modulation bandwidth is optimum. Figure 3(a) depicts the BER curves as a function of received power for the back-to-back (B2B) configuration (namely without transmission) at 2 Gbaud (black) and at 4 Gbaud (gold) respectively. The hard decision (HD) forward error correction (FEC) threshold is marked by the black dashed lines in Fig. 3. Under free-running operation (namely without feedback), we found that the BERs are much lower than the HD-FEC threshold with a PAM4 modulation rate up to 4 Gbaud. The limitation is mainly attributed to the relaxation oscillation frequency which is limited to a about 4 GHz at most.

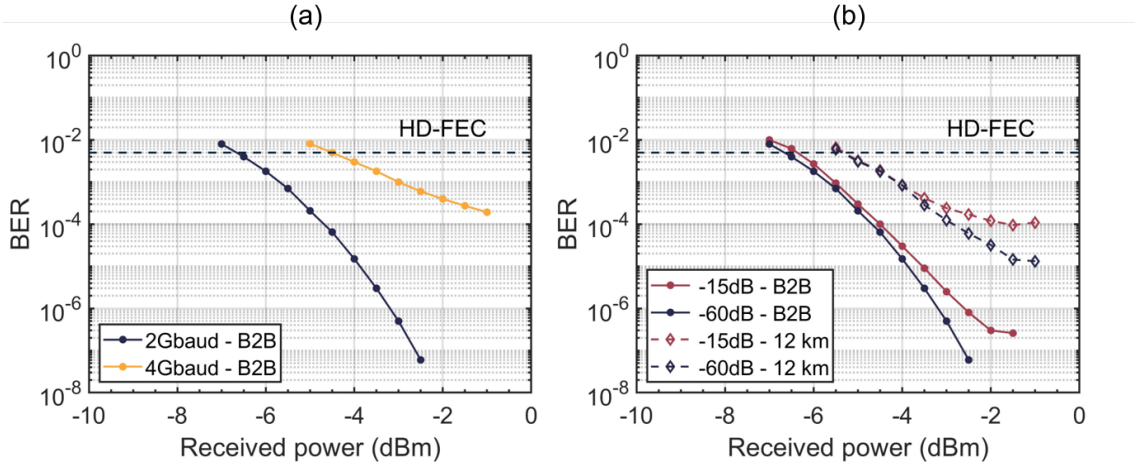

Fig. 3. (a) BER plots for back-to-back (B2B) with a PAM4 modulation rate at 2 Gbaud (gold) and 4 Gbaud (black). (b) BER plots for B2B and after 12 km transmission (12 km) under -60 dB (black) and -15 dB (burgundy) feedback strength with a PAM4 modulation rate at 2 Gbaud. The laser operates at 6 $\times I_{th}$ and 55°C.

Figure 3(b) now depicts the BER plots as a function of received power at 2 Gbaud under different feedback conditions. We analyze four cases to evaluate the feedback sensitivity of the device: with a low r_{ext} of -60 dB for the B2B (marked by black dots) and after 12 km transmission (marked by black diamond symbols) configurations, and with a strong r_{ext} of -15 dB for the B2B (marked by burgundy dots) and after 12 km transmission (marked by burgundy diamond symbols) configurations. The influence of feedback is observed from the increase of penalty. This increase is driven by two physical effects. First, the increase between the B2B without feedback and the B2B with feedback where the impact of the intensity noise due to the feedback is involved. Then, when the laser operates in transmission, the phase noise and the chirp are converted into intensity noise by the optical fiber. This results in an extra penalty of about 1.5 dB at 10^{-4} BER level. Despite that, the results show that the QD DFB laser is a reliable source against feedback. The BERs always perform below the HD-FEC threshold both in B2B and after transmission. Overall, the floor-free performance of the laser at 55°C gives insight for developing a reliable on-chip source for uncooled integrated system.

6. Conclusions

The results highlight the potential of the large optical mismatch assisted single frequency DFB laser for the development of uncooled and isolator-free high-speed photonic integrated circuits. Transmission capacity can be further improved by optimizing the laser structure in particular by considering DFBs with shorter cavity lengths.

References

1. M. Masoudi et al., Green Mobile Networks for 5G and Beyond. IEEE Access., **7**, 107270 (2019).
2. J. C. Norman et al. APL Photonics **3**, 030901 (2018).
3. M. T. Crowley et al. Semiconductors & Semimetals **86**, 371, Elsevier (2012).
4. F. Grillot et al. Nanophotonics **9**, 1271 (2020).
5. H. Nishimoto et al. J. Light. Technol. **5**, p. 1399 (1987).
6. K. Nishi et al. J. Cryst. Growth **378**, p. 459 (2013).